THE JOURNAL OF PHYSICAL CHEMISTRY LETTERS
A JOURNAL OF THE AMERICAN CHEMICAL SOCIETY

pubs.acs.org/JPCL

Letter

Unlocking Switchable Reactivity of MBene via Asymmetric Surface Adsorption

Zisheng Zhang and Frank Abild-Pedersen*

Cite This: *J. Phys. Chem. Lett.* 2025, 16, 12619−12624

Read Online

ACCESS | Metrics & More | Article Recommendations | Supporting Information

ABSTRACT: The Sabatier principle and activity volcano have guided and constrained catalyst design. Surpassing these limitations requires going beyond the static view of catalysis. Here, we propose 2D metal boride (MBene) as a promising model system for dynamic catalysis, exemplified by the nitrogen reduction reaction (N_2RR). The surface reactivity of B-rich MBene can be altered by binding organic ligands to the opposite side of the N_2RR site. The change in reactivity originates in structural distortions of the metal and boron layers, leading to an energy span of up to 0.8 eV. By cycling the ligands or running a coupled reaction on the opposite side, we could switch between under- and overbinding energetics to surpass the Sabatier limit and access the inverse activity volcano. The reactivity space considering various metals and ligands can be efficiently explored by interpretable machine learning based on geometric descriptors, and promising ligand-bound MBenes for various catalytic scenarios are proposed.

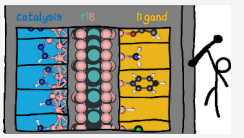

Catalysis underlies all aspects of our modern life, from plastics to medicines, and from mass chemical feedstock to renewable/sustainable technologies. However, the design of efficient catalysts suffers from an intrinsic bottleneck according to the scaling relationships and the Sabatier principle:[1,2] catalysts that bind the reactants favorably usually have difficulty desorbing the products, which blocks the active sites; while at the opposite extreme, the reactants would interact with the surface too weakly to activate in the first place. These constraints, rooted in the conservation of bond order at the surface and the intrinsic similarity among the reaction intermediates,[3] lead to the volcano-shaped relationship where the apex represents the theoretical upper limit of overall activity.[4]

To overcome such limitations, the catalysis community has employed various strategies: morphology and nanostructure engineering, heteroatom doping and high-entropy mixing, and external strain or fields.[5] However, these approaches can only cause a limited deviation from the original activity volcano, as the catalyst still operates on a more or less static surface in steady state. The past decade has seen the rise of the concept of dynamic catalysis,[6,7] which exploits the geometric, compositional, and/or electronic variation of the catalyst surface, under aggressive conditions, to alter the surface reactivity or populate an ensemble of metastable active sites.[8−10] By applying oscillating conditions, the intrinsic properties of the active site can even be altered and cycled on-the-fly, with the system operating constantly out of equilibrium with huge rate enhancement.[11] However, these approaches rely heavily on catalyst systems that are highly fluxional and responsive to changing conditions, usually (sub)nanoscale metal clusters,[12,13] whose evolving distribution of catalyst states and their properties are extremely challenging to track, let alone precisely manipulate.

Two-dimensional (2D) materials, with well-defined atomic structures and strong responses to external stimuli, have had tremendous success in electronics and electrochemical technologies.[14,15] However, they typically have an inorganic skeleton with a highly rigid structure, affording no structural fluxionality, which limits their tunability for applications that require more dramatic swings of properties than what strain or field response can offer.

In this work, we propose 2D transition metal borides (MBene,[16] also known as Boridene[17]) as a promising platform for dynamic catalysis. Owing to its unique three-valence-electron configuration, boron is capable of forming exotic chemical bonds and diverse structural motifs in its allotropes,[18] compounds,[19] and surface arrangements.[20] These motifs have been shown to dictate the chemistry of borides in various thermal and electrocatalytic reactions, with the metal component often playing a minor role.[21−23] Furthermore, as a semimetal, boron exhibits affinity toward organic functionalization, offering an additional layer of tunability.[24] Because of the favorable energy level and symmetry matching between the frontier orbitals of B and the antibonding orbitals of N_2,[25−27] we focus on the nitrogen reduction reaction (N_2RR) to ammonia − one of the most Sabatier-limited catalytic processes,[28] yet an ideal case for showcasing the potential of dynamic catalysis.

The specific MBene this work investigates is the α diboride-derived structure, which features sandwich-like alternating layers of transition metal and boron.[29] The boron layers feature a hexagonal lattice with highly delocalized multicenter

Received: October 10, 2025
Revised: November 17, 2025
Accepted: November 21, 2025
Published: December 2, 2025

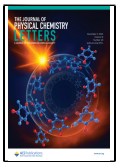

https://doi.org/10.1021/acs.jpclett.5c03160
J. Phys. Chem. Lett. 2025, 16, 12619−12624

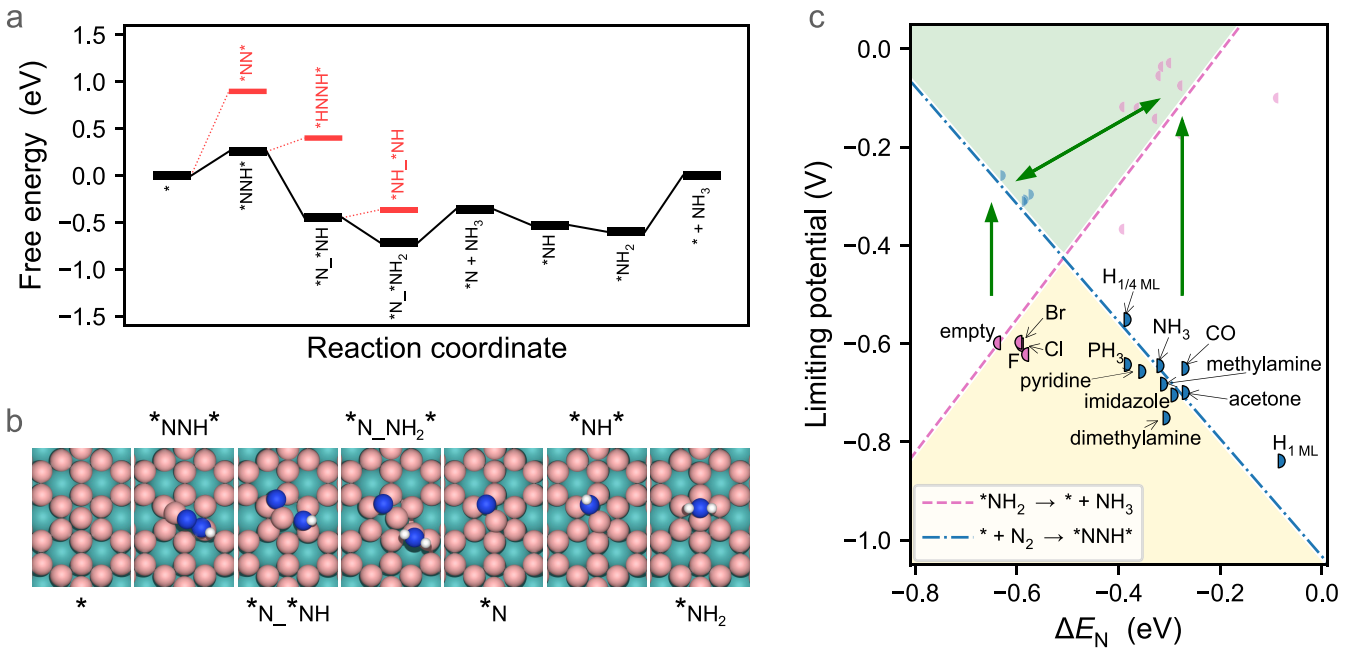

Figure 1. Nitrogen reduction reaction on MBene. (a) Free energy diagram of N_2RR on 2D Mo boride at the equilibrium potential of the N_2RR, with unfavorable pathways shown in red. (b) Geometries of the N_2RR intermediates, color code: H − white, N − blue, B − pink, Mo − cyan. (c) Activity volcano of N_2RR with binding energy of N as the descriptor. All potential values are referenced against the equilibrium potential of N_2RR.

chemical bonding in-plane.[30] Depending on the synthetic conditions, the B_6 hexagons on the surface can be partially filled at the centers by excess B, forming slightly buckled B_7 units.[31] Although the boron layer is overall anionic, the center B site is positively charged and can serve as a Lewis acid site (Figure S3).

We first investigate the N_2RR mechanism on the Mo MBene surface, with the free energy diagram shown in Figure 1a and the geometry of reaction intermediates shown in Figures 1b and S1−S2. Since N_2 is a weak Lewis base, it can weakly coordinate atop the center B site with a binding energy of −0.08 eV. However, it would not readily activate at this point due to boron's lack of back-donating electrons. The first hydrogenation step is slightly uphill with a ΔG of +0.26 eV, which activates the N−N bond and enables it to bridge over the B_7 moiety in a side-on configuration. The activated NNH can then readily dissociate into *N and *NH, both residing on trifold sites on the B_7 unit (ΔG = −0.71 eV). The next hydrogenation step takes place on the *NH and is downhill with a ΔG of −0.26 eV. The desorption of the first NH_3, however, is uphill by +0.35 eV. The remaining *N can also be readily hydrogenated but is difficult to remove, and the whole reaction is limited by the final desorption step from $*NH_2$ to NH_3 (g). Hence, the pristine 2D Mo boride falls on the overbinding leg (left leg in Figure 1c) of the N_2RR activity volcano, where the overall kinetics are limited by product desorption, with a limiting potential of −0.6 V.

Inspired by the sandwich-like structure of the MBene, which closely resembles organometallic complexes with metal-to-ring η-bonding modes, we functionalize the opposite side of the MBene (as opposed to the N_2RR side, referred to as the *bottom*, see Figure S5) and probe its influence on the reactivity of the *top* surface (representative ligands in Figure 2, full library in Figure S8). Surprisingly, hydrogen adsorption on the bottom surface can weaken N_2 activation by up to 0.58 eV and facilitate NH_3 desorption by 0.50 eV, i.e., the Mo MBene is

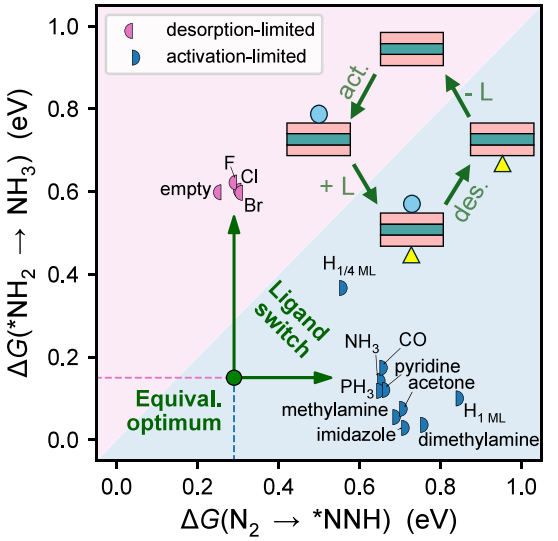

Figure 2. Ligand-dependent surface reactivity of 2D boride. The optimal cycling path in the reactivity space is marked by green arrow. The inset shows the schematics of a switching cycle coupled with a catalytic cycle.

transformed from an overbinding catalyst into an underbinding one upon hydrogen adsorption (Figure S4). The hydride state on the bottom surface can be easily prepared or removed by reducing agents or mild oxidants (or hydride scavengers), respectively, so that the reactivity of the MBene can be switched between the activation- and desorption-limited regimes, i.e., between the left and right legs of the N_2RR activity volcano (Figures 1c and S6, S7, S9).

Since dynamic catalysis relies on rapid switching of catalyst states, conventional organic functionalizations via electron-withdrawing/donating groups are unsuitable. Hence, we limit our scope to Lewis bases, which can form dative bonds with

https://doi.org/10.1021/acs.jpclett.5c03160
J. Phys. Chem. Lett. 2025, 16, 12619−12624

the center B site (Lewis acidic) and are relatively easy to remove. The impact of halides is negligible, while CO, NH_3, and PH_3 alter the free energetics by about 0.4 eV, following the same trendline as defined by the hydride cases. Larger organic bases (primary and secondary alkylamines, pyridine, imidazole, and acetone) cause greater changes, weakening activation by up to 0.49 eV and facilitating desorption by up to 0.54 eV. To restore the system to the empty state, the bound Lewis bases can be scavenged by supplying a catalytic amount of Lewis acid molecules.

Here we pause to discuss the potential realization of this catalytic system. The 2D catalyst can be prepared as a film and placed between two separate chambers: the control chamber and the catalysis chamber. The catalysis chamber is where reactants are supplied, while the control chamber is responsible for switching the ligand on the bottom side of the catalyst film. The control may be achieved via gas-phase chemistry, by alternating the atmosphere between hydrogenating and mildly oxidative (gas composition pulses). In the liquid phase, it could be realized by pumping dissolved Lewis acids and bases to flush the bottom surface alternately within a microfluidics system. It could also be controlled electrochemically, by applying potential pulses to switch a redox-active molecule between the oxidized acidic state and the reduced basic state, similar to a pH-swing system. In all cases, the concept should be realizable on a chip-scale device. Scaling to larger scale applications, however, would require more careful reactor design and engineering considerations, which are beyond the scope of this Letter. If the ligand state of the bottom surface can be switched at the characteristic frequency of N_2RR, then the top surface of the catalyst would operate as overbinding to activate N_2 before switching and under-binding to trigger NH_3 desorption after switching (Figure 2 inset). However, the turnover frequency in this case would be limited by the frequency of ligand switching.[32]

Alternatively, we may utilize the chemical symmetry and communication between the top and bottom surfaces of the MBene and have another catalytic reaction running in the control chamber in parallel. This would avoid the need to apply any pulses throughout the reaction, and there are two possible realizations: (1) we could run a different hydrogenation reaction in the control chamber, so that empty−*H cycling during the catalysis can switch the activity in the top side for the catalysis chamber; (2) or, since both NH_3 and H can act as reactivity-altering ligands, we envision running N_2RR on both sides but with the two catalysis chambers operating out-of-phase (in terms of the stage in a catalytic cycle), so that reaction progress would intrinsically drive the ligand switching for both sides at the characteristic time scale of N_2RR. The initial out-of-phase state may be induced by a lag time between the reactant feeding into top and bottom chambers, or by differing the gas composition (N-richer and H-richer). Ideally, both cases would be equivalent to operating in the "inverse" volcano (Figures 1c and S9).

To understand the origin of the unexpectedly large energy span unlocked via simple Lewis adduct on the other side of the catalytic surface, we examined the adsorption configurations in the presence of reaction intermediates or ligands. Figure 3 shows the structural distortion of the top and middle layers along the surface normal direction in various scenarios. Different adsorbates lead to significantly different extents of distortion in the top and middle layers, which are linked to their binding modes: atop-mode adsorbates (N_2, NH_3, H, and

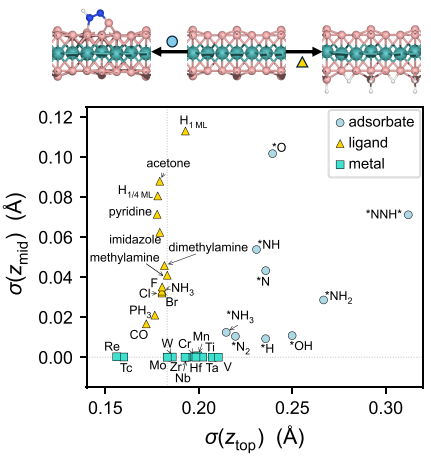

Figure 3. Structural distortion of the MBene in cases of various adsorbates, ligands, and metals. The values corresponding to the bare Mo MBene is marked by dotted lines. Side views of representative structures with significant top- and middle-layer distortion is shown above the plot.

OH) only slightly elevate the center B while keeping the middle metal layer almost unchanged; adsorbates with trifold (*N, *NH), bridge (*O, *NH_2), or multidentate (*NNH*) modes, however, greatly deform the hexagonal lattice of the top surface, competing with surface B for its valence electrons in the conjugated system and partially breaking surface B−B bonds. The bottom-surface ligands (full library in Figure S10), although they cannot influence the top surface much due to a lack of direct chemical interaction, can significantly distort the middle metal layer. In other words, the bottom-surface ligands and the top-surface adsorption energetics are coupled through the structural distortion of the middle layer. This also explains the relatively poor correlation among the adsorption energies of some N_2RR intermediates. By changing the metal component of the MBene, the surface B layer can be distorted depending on the lattice parameters imposed by the metal component, causing different extents of B_7 buckling on the top surface while keeping the middle layer flat, thereby offering an orthogonal direction of optimization. Note that this is not purely a strain effect: applying in-plane tensile or compressive strain does not induce variations in reaction free energies or surface B distortions as large as those achieved by changing the metal component (Figure S11).

After considering different metal elements, the reactivity space expands to $N_{metal} \times N_{ligand} \times N_{adsorbate}$ adsorption systems, which scales as N^3 and is prohibitively expensive for an explicit and exhaustive exploration. To overcome this, we employ machine learning for low-cost prediction of adsorption free energies. Guided by the insights in Figure 3, we hypothesize that the geometric distortions of the top and middle layers are sufficient to capture the essence and coupling of adsorbate-metal−ligand interactions. Accordingly, we construct a set of primarily geometry-based descriptors[33] to train the model: key bond lengths, interlayer distances, and the distortion metrics in Figure 3. The computational cost for generating these inputs scales only as $3N$. The resulting model accurately predicts adsorption free energies on both training and test sets (Figure 4a), demonstrating strong generalization and confirming that geometric metrics suffice to represent the underlying chemistry of MBenes. SHAP analysis further interprets the model's predictions, highlighting interlayer

https://doi.org/10.1021/acs.jpclett.5c03160
J. Phys. Chem. Lett. 2025, 16, 12619−12624

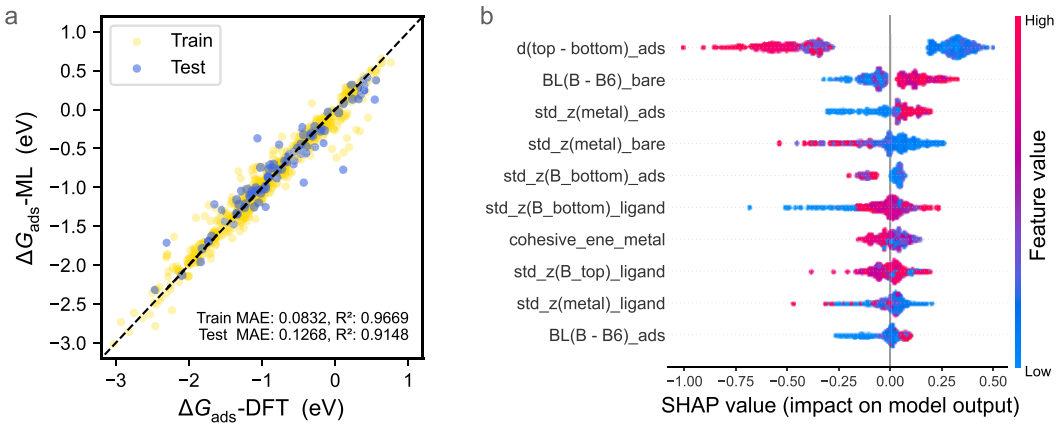

Figure 4. Interpretable machine learning of adsorption free energetics based on simple geometric descriptors. (a) The parity plot showing the correlation between DFT-computed and ML-predicted adsorption free energies. (b) SHAP summary plot showing the relative importance and impact of geometric descriptors on the ΔG_{ads} prediction.

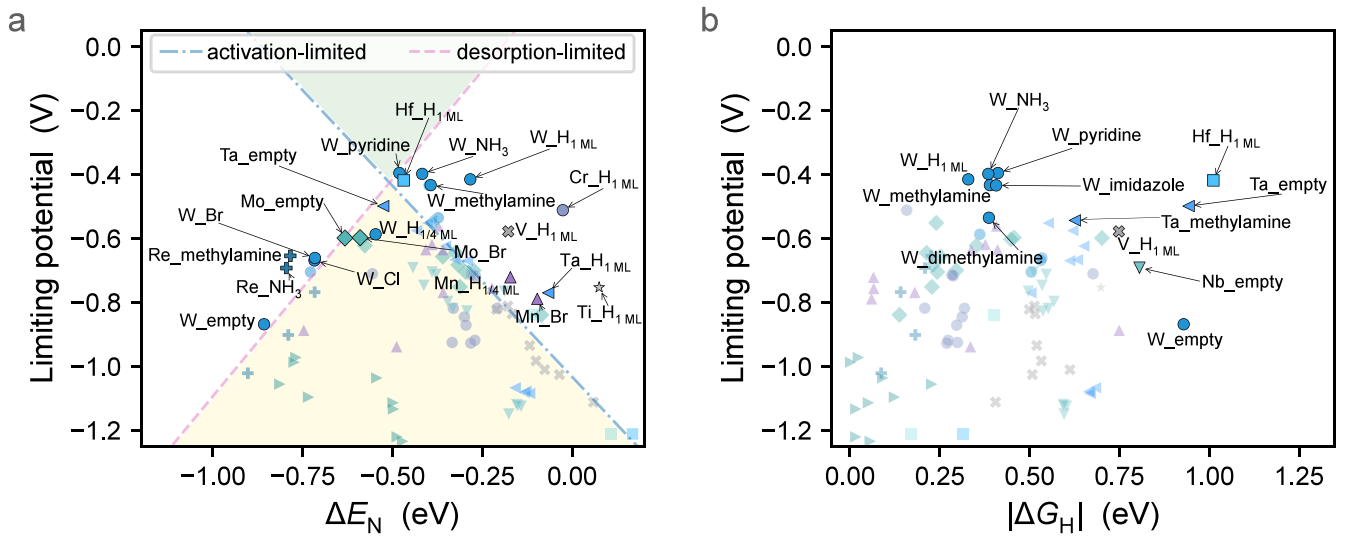

Figure 5. Exploration of the reactivity space spanned by different metal component and ligand types in MBene. (a) Search toward optimal N_2RR limiting potential, with promising candidatesfor direct use or switchable setup highlighted. (b) Pareto search for candiates with optimal N_2RR activity and minimal HER activity. The searches are performed using the ML model, followed by DFT confirmation. All final values shown herein are DFT-computed.

expansion, deformation at the B_7 moiety, and structural distortions of the middle/bottom layers as the most important features (Figure 4b). We have also trained the ML model with additional Bader charge-based features, however, there is no improvement of the performance, and SHAP analyses (Figure S12) show that the top three most important features are all geometry-based. The most important Bader charge descriptor has only about one-quarter of the importance of the leading geometric feature. This reassures the dominance of geometric factors in determining the reactivity of the surface B layer, which is quite advantageous in that we can accurately predict reaction free energetics solely from energy-minimum geometry, which greatly reduces the overall computational cost of feature evaluation.

The fitted ML model is then used to search the reactivity space for a pool of optimal candidates, which is then refined and confirmed with DFT. The first search aims to locate the candidates with the highest ΔG in all N_2RR steps (Figure 5a). The data points largely fall within the activity volcano as in Figure 1c, with a few outliers on the right-leg side due to strong structural distortion from heavy hydriding of strained MBenes. For a switchable dynamic catalysis setup, the goal is to locate a pair of ligand states that are on different legs of the activity volcano and as far apart as possible. The optimal systems in this case are the empty-hydride pair for W MBene, the empty-bromide pair for Mn MBene, and the empty-hydride pair for Mo MBene.

For N_2RR in a conventional reactor, the ligand-bound W MBenes are the optimal group, with hydride-bound Hf MBene, hydride-bound Cr MBene, and empty Ta MBene also in the competitive pool. However, in a conventional reactor with protic solvent, hydrogen evolution reaction (HER) is a major side reaction. In Figure 5b, we perform a Pareto search to optimize N_2RR while suppressing HER (maximize $|\Delta G_H|$) and show the candidates within the first three Pareto frontiers. The W and Mo MBenes, despite having high N_2RR activity, are more prone to HER. In fact, MoB_2 is known as an active HER catalyst.[29] The Hf and Ta MBene can minimize HER without compromising N_2RR.

https://doi.org/10.1021/acs.jpclett.5c03160
J. Phys. Chem. Lett. 2025, 16, 12619−12624

In summary, we propose MBenes as a promising model catalyst for dynamic catalysis, featuring structural flexibility, strong coupling between the top and bottom surface layers, and modification of surface properties via organic ligands. By switching the bound ligand, the working surface of the catalyst can swing between overbinding and under-binding states along the scaling relationship by up to 0.6 eV, operating on the "inverse" activity volcano at ideal oscillating frequencies. This reactivity-switching on MBene is agnostic to the catalyzed reaction and can be generalized to other multistep reducing reactions, such as the CO_2 reduction reaction (Figure S13), with a similar energy span. We further demonstrate that the switchable surface chemistry can be well captured by a set of geometric descriptors, enabling interpretable machine learning for accurate prediction of adsorption free energies and low-cost exploration of the vast metal−ligand-adsorbate reactivity space. We provide a generalizable workflow and highlight the opportunities at the interface between (in)organic chemistry and material science for designing model catalysts with highly tunable reactivity.

■ ASSOCIATED CONTENT

Data Availability Statement

All DFT-computed structures and energetics are available on the catalysis-hub.org repository.[34]

Supporting Information

The Supporting Information is available free of charge at https://pubs.acs.org/doi/10.1021/acs.jpclett.5c03160.

Computational details of the DFT calculations and ML models; structures of all reaction intermediates of unfavorable and favorable N_2RR pathways; Bader charges of surface B atoms in the presence of bottom side adsorbates; comparison of N_2RR free energy diagrams of empty and hydride states; structures of the MBenes with different ligands; fitted scaling relations of N_2RR steps and overall energetics (PDF)

Transparent Peer Review report available (PDF)

■ AUTHOR INFORMATION

Corresponding Author

Frank Abild-Pedersen − *SUNCAT Center for Interface Science and Catalysis, SLAC National Accelerator Laboratory, Menlo Park, California 94025, United States;* orcid.org/0000-0002-1911-074X; Email: abild@slac.stanford.edu

Author

Zisheng Zhang − *SUNCAT Center for Interface Science and Catalysis, SLAC National Accelerator Laboratory, Menlo Park, California 94025, United States; Department of Chemical Engineering, Stanford University, Stanford, California 94305, United States;* orcid.org/0000-0002-4370-4038

Complete contact information is available at: https://pubs.acs.org/10.1021/acs.jpclett.5c03160

Notes

The authors declare no competing financial interest.

■ ACKNOWLEDGMENTS

Z.Z. is supported by the Stanford Energy Fellowship from the Precourt Institute for Energy, Doerr School of Sustainability. F.A-P. acknowledges support from the U.S. Department of Energy, Office of Science, Office of Basic Energy Sciences, Chemical Sciences, Geosciences, and Biosciences Division, Catalysis Science Program to the SUNCAT Center for Interface Science and Catalysis. Computational facilities used to conduct this study include: S3DF, SLAC Shared Scientific Data Facility; Sherlock, a university-shared computing cluster operated by Stanford Research Computing Center; National Energy Research Scientific Computing Center, a DOE Office of Science User Facility supported by the Office of Science of the U.S. Department of Energy under Contract No. DE-AC02-05CH11231 using NERSC award BES-ERCAP0024127. Z.Z. thanks Thomas F. Jaramillo, Michal Bajdich, and Kirsten Winther for helpful discussions and assistance in uploading datasets to Catalysis-Hub.

■ REFERENCES

(1) Abild-Pedersen, F.; Greeley, J.; Studt, F.; Rossmeisl, J.; Munter, T. R.; Moses, P. G.; Skúlason, E.; Bligaard, T.; Nørskov, J. K. Scaling Properties of Adsorption Energies for Hydrogen-Containing Molecules on Transition-Metal Surfaces. *Phys. Rev. Lett.* **2007**, *99*, 16105−16105.

(2) Medford, A. J.; Vojvodic, A.; Hummelshøj, J. S.; Voss, J.; Abild-Pedersen, F.; Studt, F.; Bligaard, T.; Nilsson, A.; Nørskov, J. K. From the Sabatier Principle to a Predictive Theory of Transition-Metal Heterogeneous Catalysis. *J. Catal.* **2015**, *328*, 36−42.

(3) Abild-Pedersen, F.; Bligaard, T.; Rossmeisl, J.; Greeley, J. Tribute to Jens K. Nørskov. *J. Phys. Chem. C* **2025**, *129*, 1025−1026.

(4) Bligaard, T.; Nørskov, J. K.; Dahl, S.; Matthiesen, J.; Christensen, C. H.; Sehested, J. The Brønsted-Evans-Polanyi Relation and the Volcano Curve in Heterogeneous Catalysis. *J. Catal.* **2004**, *224*, 206−217.

(5) Pérez-Ramírez, J.; López, N. Strategies to Break Linear Scaling Relationships. *Nature Catalysis* **2019**, *2*, 971−976.

(6) Jung, S.; Pizzolitto, C.; Biasi, P.; Dauenhauer, P. J.; Birol, T. Programmable Catalysis by Support Polarization: Elucidating and Breaking Scaling Relations. *Nat. Commun.* **2023**, *14*, 7795.

(7) Jangid, P.; Chaudhury, S.; Kolomeisky, A. Theoretical Understanding of Dynamic Catalysis. *J. Phys. Chem. C* **2024**, *128*, 9077−9089.

(8) Zhang, Z.; Zandkarimi, B.; Alexandrova, A. N. Ensembles of metastable states govern heterogeneous catalysis on dynamic interfaces. *Accounts of chemical research* **2020**, *53*, 447−458.

(9) Lavroff, R. H.; Morgan, H. W.; Zhang, Z.; Poths, P.; Alexandrova, A. N. Ensemble representation of catalytic interfaces: soloists, orchestras, and everything in-between. *Chemical science* **2022**, *13*, 8003−8016.

(10) Alexandrova, A. N.; Christopher, P. Heterogeneous Catalysis: Optimal Performance at a Phase Boundary? *Matter* **2025**, *8*, 102209.

(11) Dauenhauer, P. J. Up up down down Left Right Left Right B A Start for the Catalytic Hackers of Programmable Materials. *Matter* **2023**, *6*, 4145−4157.

(12) Zhang, Z.; Zandkarimi, B.; Munarriz, J.; Dickerson, C. E.; Alexandrova, A. N. Fluxionality of Subnano Clusters Reshapes the Activity Volcano of Electrocatalysis. *ChemCatChem* **2022**, *14*, No. e202200345.

(13) Oh, K.-R.; Walton, A.; Chalmers, J. A.; Hopkins, J. A.; Canavan, J. R.; Onn, T. M.; Scott, S. L.; Frisbie, C. D.; Dauenhauer, P. J. Alumina−Titania Nanolaminate Condensers for Hot Programmable Catalysis. *ACS Materials Letters* **2024**, *6*, 3478−3486.

(14) Chia, X.; Pumera, M. Characteristics and Performance of Two-Dimensional Materials for Electrocatalysis. *Nature Catalysis* **2018**, *1*, 909−921.

(15) Zhang, M.; Wang, Z.; Bo, X.; Huang, R.; Deng, D. Two-Dimensional Catalysts: From Model to Reality. *Angew. Chem., Int. Ed.* **2025**, *64*, No. e202419661.

(16) Jin, S.; Shi, Z.; Wang, R.; Guo, Y.; Wang, L.; Hu, Q.; Liu, K.; Li, N.; Zhou, A. 2D MoB MBene: An Efficient Co-Catalyst for Photocatalytic Hydrogen Production under Visible Light. *ACS Nano* **2024**, *18*, 12524−12536.
(17) Zhou, J.; Palisaitis, J.; Halim, J.; Dahlqvist, M.; Tao, Q.; Persson, I.; Hultman, L.; Persson, P. O. Å.; Rosen, J. Boridene: Two-dimensional Mo4/3B2-x with Ordered Metal Vacancies Obtained by Chemical Exfoliation. *Science* **2021**, *373*, 801−805.
(18) Oganov, A.; Solozhenko, V. Boron: a hunt for superhard polymorphs. *Journal of Superhard Materials* **2009**, *31*, 285−291.
(19) Li, W.-L.; Chen, X.; Jian, T.; Chen, T.-T.; Li, J.; Wang, L.-S. From planar boron clusters to borophenes and metalloborophenes. *Nature Reviews Chemistry* **2017**, *1*, 0071.
(20) Li, H.; Ruan, Q.; Lamarca, C.; Tsui, A.; Yakobson, B. I.; Hersam, M. C. Atomic-Resolution Structural and Spectroscopic Evidence for the Synthetic Realization of Two-Dimensional Copper Boride. *Sci. Adv.* **2025**, *11*, No. eadv8385.
(21) Venegas, J. M.; McDermott, W. P.; Hermans, I. Serendipity in catalysis research: boron-based materials for alkane oxidative dehydrogenation. *Accounts of chemical research* **2018**, *51*, 2556−2564.
(22) Park, H.; Encinas, A.; Scheifers, J. P.; Zhang, Y.; Fokwa, B. P. Boron-dependency of molybdenum boride electrocatalysts for the hydrogen evolution reaction. *Angew. Chem., Int. Ed.* **2017**, *56*, 5575−5578.
(23) Lee, E.; Park, H.; Joo, H.; Fokwa, B. P. Unexpected Correlation Between Boron Chain Condensation and Hydrogen Evolution Reaction (HER) Activity in Highly Active Vanadium Borides: Enabling Predictions. *Angewandte Chemie - International Edition* **2020**, *59*, 11774−11778.
(24) Alexandrova, A. N.; Boldyrev, A. I.; Zhai, H. J.; Wang, L. S. All-Boron Aromatic Clusters as Potential New Inorganic Ligands and Building Blocks in Chemistry. *Coord. Chem. Rev.* **2006**, *250*, 2811−2866.
(25) Légaré, M.-A.; Bélanger-Chabot, G.; Dewhurst, R. D.; Welz, E.; Krummenacher, I.; Engels, B.; Braunschweig, H. Nitrogen Fixation and Reduction at Boron. *Science* **2018**, *359*, 896−900.
(26) Liu, C.; Li, Q.; Wu, C.; Zhang, J.; Jin, Y.; Macfarlane, D. R.; Sun, C. Single-Boron Catalysts for Nitrogen Reduction Reaction. *J. Am. Chem. Soc.* **2019**, *141*, 2884−2888.
(27) Liu, X.; Jiao, Y.; Zheng, Y.; Qiao, S. Z. Isolated Boron Sites for Electroreduction of Dinitrogen to Ammonia. *ACS Catal.* **2020**, *10*, 1847−1854.
(28) Logadottir, A.; Rod, T.; Nørskov, J.; Hammer, B.; Dahl, S.; Jacobsen, C. The Brønsted−Evans−Polanyi Relation and the Volcano Plot for Ammonia Synthesis over Transition Metal Catalysts. *J. Catal.* **2001**, *197*, 229−231.
(29) Jothi, P. R.; Zhang, Y.; Scheifers, J. P.; Park, H.; Fokwa, B. P. T. Molybdenum diboride nanoparticles as a highly efficient electrocatalyst for the hydrogen evolution reaction. *Sustainable Energy Fuels* **2017**, *1*, 1928−1934.
(30) Park, H.; Zhang, Y.; Scheifers, J. P.; Jothi, P. R.; Encinas, A.; Fokwa, B. P. Graphene-and phosphorene-like boron layers with contrasting activities in highly active Mo2B4 for hydrogen evolution. *J. Am. Chem. Soc.* **2017**, *139*, 12915−12918.
(31) Zhang, Z.; Abild-Pedersen, F. Off-Equilibrium Reactivity of Boron-Enriched Metal Diboride Surfaces in Electroreduction Conditions. *ACS Catal.* **2025**, *15*, 12340−12350.
(32) Canavan, J. R.; Hopkins, J. A.; Foley, B. L.; Abdelrahman, O. A.; Dauenhauer, P. J. Catalytic Resonance Theory: Turnover Efficiency and the Resonance Frequency. *ACS Catal.* **2025**, *15*, 653−663.
(33) Zhang, Z.; Hermans, I.; Alexandrova, A. N. Off-stoichiometric Restructuring and Sliding Dynamics of Hexagonal Boron Nitride Edges in Conditions of Oxidative Dehydrogenation of Propane. *J. Am. Chem. Soc.* **2023**, *145*, 17265−17273.
(34) Winther, K. T.; Hoffmann, M. J.; Boes, J. R.; Mamun, O.; Bajdich, M.; Bligaard, T. Catalysis-Hub. org, an open electronic structure database for surface reactions. *Sci. Data* **2019**, *6*, 75.

https://doi.org/10.1021/acs.jpclett.5c03160
J. Phys. Chem. Lett. 2025, 16, 12619−12624